Green Electrochemical Template Synthesis of CoPt Nanoparticles with Tunable Size, Composition and Magnetism from Microemulsions Using an Ionic Liquid ($bmimPF_6$)

Albert Serrà [1], Elvira Gómez [1], José Francisco López-Barbera [2] Josep Nogués [2,3], Elisa Vallés [1,]*

[1] Departament *de Química Física and Institut de Nanociència i Nanotecnologia (IN²UB), Universitat de Barcelona, Martí i Franquès 1, 08028, Barcelona, Spain.*

[2] *ICN2 - Institut Català de Nanociència i Nanotecnologia, Campus UAB, 08193 Bellaterra (Barcelona), Spain.*

[3] *ICREA - Institució Catalana de Recerca i Estudis Avançats, Barcelona, Spain*.

Corresponding Author

e.valles@ub.edu

Abstract

Electrodeposition from microemulsions using ionic liquids is revealed as a method for synthesizing magnetic alloyed nanoparticles, avoiding the use of aggressive reducing agents. Microemulsions containing droplets of aqueous solution (electrolytic solution containing Pt(IV) and Co(II) ions) in an ionic liquid ($bmimPF_6$) define nanoreactors in which the electrochemical reduction takes place. Highly crystalline hcp alloyed CoPt nanoparticles, in the 10-120 nm

range with a rather narrow size distribution, have been deposited on a conductive substrate. The relative amount of aqueous solution to ionic liquid determines the size of the nanoreactors, which serve as nanotemplates for the growth of the nanoparticles and hence determine their size and distribution. Further, the stoichiometry (Pt_xCo_{1-x}) of the particles can be tuned by the composition of the electrolytic solution inside the droplets. The control of the size and composition of the particles allows tailoring the room temperature magnetic behavior of the nanoparticles from superparaparamagnetic to hard-magnetic (with a coercivity of H_C = 4100 Oe) in the as-obtained state.

Keywords: Ionic Liquid, CoPt nanoparticles, Electrodeposition, Microemulsions, Magnetism.

Nanoparticles have numerous potential applications in catalysis,[1,2] biological labeling,[3,4] photonics,[5,6] optoelectronics,[7] integration in micro/nanoelectromechanical systems,[8,9] and information storage,[10,11] among others, due to their extraordinary physical and chemical properties. Shape, composition, size and size distribution of the nanoparticles are the key factors that condition their properties and determine their potentialities.[12–14] Therefore, the synthesis of nanoparticles of customized size and shape has long been a scientific and technological challenge. [15–17]

The use of microemulsions is a significant synthesis method to prepare homogeneous and monodisperse small nanoparticles of metals, metal oxides and other inorganic materials.[18–22] Classical microemulsions are systems composed of water (W), oil (O), and surfactant (S), which are a single thermodynamically stable and optically isotropic liquid phase.[23,24] The most usual synthesis pathway is performed in water droplets of a few nanometers, which act as nanoreactors, stabilized by surfactant in a continuous oil medium. The nanoreactors limit the size and size distribution of the synthesized particles according to the size and size distribution of the droplets. Nanoparticle formation results from the reactions initiated by chemical reducing agents,[25–28] which are generally rather aggressive. However, to avoid the use of chemical reducing agents, the direct reduction of ions in the aqueous component of the microemulsion by electrodeposition has been recently proposed as an alternative.[29-31] Notably, electrodeposition

offers both economic and environmental benefits because it is simple, easily scalable, it implies low setup costs and avoids the use of aggressive chemical reducing agents. Nevertheless, electrodeposition from microemulsions is limited by the high ohmic resistance of the dielectric (oil) component in the microemulsion.

In the last decades, ionic liquids (ILs) and deep-eutectic solvents (DES) have been suggested as interesting media for electrodeposition due to their intrinsic ionic conductivity, low vapor pressure, high dissolution properties and wide electrochemical window.[32-34] Recently, some studies have reported that ionic liquids may substitute either water or oil in classical microemulsions.[35-37] For example, water-in-ionic liquid (W/IL) microemulsions can be prepared using ionic liquids instead of organic solvents in the presence of an adequate surfactant.[38-42] Such novel microemulsions systems have both the advantages of ionic liquids and conventional microemulsions. The advantages of choosing IL instead of a classical organic solvent are the higher conductivity of the ionic liquid compared to an organic solvent, which increases the conductivity of the microemulsion, allowing significantly higher deposition rates. Moreover, ionic liquids are considered green solvents because they are not volatiles with very low vapor pressure and non-inflammable. Also, the high viscosity of the ionic liquids can favor the non-coalescence of the droplets of aqueous solution.

Here we demonstrate the synthesis of alloyed magnetic nanoparticles using water-in-ionic liquid microemulsions by electrodeposition, thus avoiding the use of reducing reagents. Alloyed CoPt nanoparticles of different sizes, in the range of 10-120 nm, have been electrochemically synthesized using different W/IL/S (CoPt aqueous solution/ bmimPF_6/ Triton X-100) microemulsions. The amount of CoPt aqueous solution in the microemulsion permits the control of the nanoreactor size, allowing the synthesis of hcp CoPt nanoparticles of different sizes. Further, the stoichiometry of the nanoparticles is directly controlled by the Co/Pt ratio in the nanoreactors. The size and composition of the nanoparticles is shown to determine their magnetic behavior.

RESULTS AND DISCUSSION

To understand how the solubility of electroactive species in ionic liquid ($bmimPF_6$**)** might affect the process, electrodeposition tests in this ionic liquid (IL) and in the ionic liquid-surfactant (IL-S) mixture were performed.

Electrodeposition Test of Cobalt-Platinum in $BmimPF_6$ (IL) and $BmimPF_6$ (IL) −Triton X-100 (S) Mixture

Although the aim was to prepare the CoPt solution in the IL with the same composition that in the microemulsion, unfortunately we could only dissolve the Pt salt (easy solubilization) and the Co salt (poor solubility) in the IL, due to the limited solubility of NH_4Cl and H_3BO_3 in the $bmimPF_6$. Therefore, the CoPt solution in IL (IL solution) contains 1.2 mM Na_2PtCl_6 and 2.5 mM $CoCl_2$ in $bmimPF_6$, after two days of solution in stirring conditions. The solution containing the non-ionic surfactant Triton X-100 (IL-S solution) was 59.4 wt. % of $bmimPF_6$ (containing 1.2 mM Na_2PtCl_6 and 2.5 mM $CoCl_2$, concentrations referred to ionic liquid volume) and 40.6 wt. % of Triton X-100. The electrodeposition of CoPt from both solutions was voltammetrically studied on a Si/Ti/Au electrode at a potential scan rate of 50 $mV \cdot s^{-1}$ under stationary conditions at room temperature (25 ºC).

Figure 1a allows detecting different electrochemical processes on the electrode. The voltamogram was started at 0.5 V, scanning first to negative potentials: three reduction processes (R_A, R_B and R_C) were recorded during the negative scan, followed by three oxidation peaks (O_D, O_E and O_F) in the positive scan. Different experiments were performed in order to assign each one of the peaks:

The oxidation peak O_F also appears when the scan was performed from 0.5 V to positive potentials (figure 1a.f1) and it corresponds to the surface oxidation of the Au seed-layer of the substrate. This peak does not appear when the voltammetry was performed on a vitreous carbon electrode (figure 1a.f2). The reduction of the Au surface oxides was observed in the R_G peak.

R_A and R_B peaks were similar to those observed for Pt (IV) reduction in other IL[43], assigned respectively to Pt (IV) to Pt (II) reduction (R_A) and Pt (II) to Pt (0) reduction (R_B). The surface

oxidation of the deposited Pt seems to occur in the O_E peak: When the scan was performed until -0.50 V and held at this potential during 0, 25 and 55 s before scanning in the reverse direction, no changes were observed in the peak O_E. However, when the scan was performed up to -1.0 V and held at this potential 0, 50, and 88 s before scanning in the reverse direction, peak O_E increased (figure 1a.e1, 88 s, and figure 1a.e2, 50 s), revealing increased Pt deposition. These facts corroborate that the first step of Pt (IV) reduction occurs during R_A and the second one, to Pt (0), occurs during R_B, being the oxidation peak O_E the one corresponding to Pt surface oxidation.

In order to assign the cathodic peak R_C and the anodic one O_D voltammograms from the initial potential up to -1.75 V were performed; this potential was held during 0, 50 and 88 s, maintaining stirring during the hold, and after the potential was scanned to positive values to analyse the peak O_D. The oxidation peak O_D appears in all cases, revealing that Co codeposits with Pt during R_C with the simultaneous discharge of the medium. We assign the peak O_D to CoPt alloy oxidation due to the significant increase observed when we apply the described holding (figure 1a.d1, 88 s, and 1a.d2, 50 s).

Concerning the CoPt system in the presence of surfactant (IL-S solution), the current density was smaller than in the IL medium indicating a lower deposition rate due to the adsorption of surfactant on the substrate and the deposit during its formation (figure 1b). In addition, surfactant adsorption could introduce changes in the intrinsic characteristics of the double layer and other interfacial phenomenon like dielectric constant, potential and current density distribution, interfacial energy, among others, that might modify the layer growth.[44–46] Both cathodic and anodic processes were identified according the previous strategy used in the IL medium.

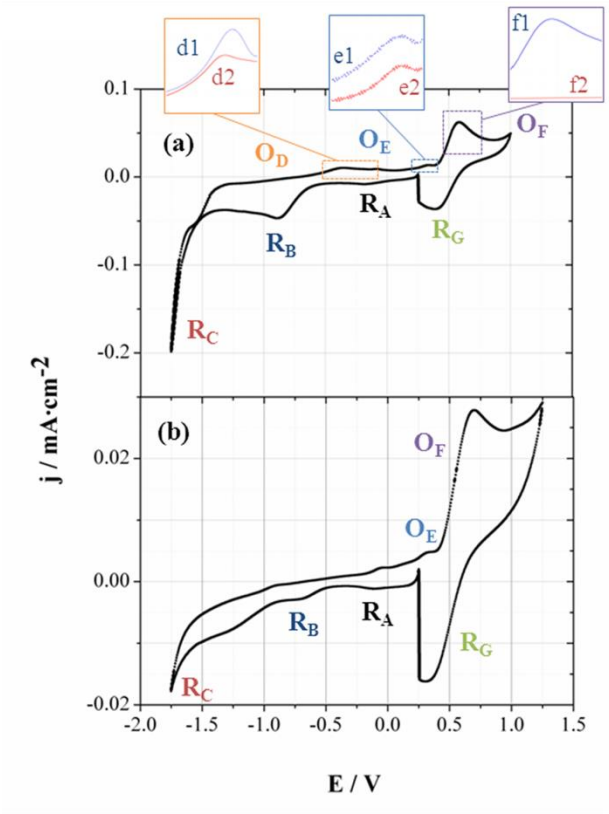

Figure 1: Cyclic voltammetry under stationary conditions at 50 mV·s^{-1} of (a) 1.2 mM Na_2PtCl_6 + 2.5 mM $CoCl_2$ in IL solution and (b) IL-S system containing 59.4 wt. % of 1.2 mM Na_2PtCl_6 and 2.5 mM $CoCl_2$ in IL solution and 40.6 wt. % of Triton X-100.

The voltammetric study revealed that it is possible to deposit CoPt from both types of IL solutions, but at very negative potentials and with low current densities. A potential of -1.75 V was necessary to perform the electrodeposition (Figure 2a) although the involved current density was low (curve A), especially in the presence of surfactant (curve B). Under these conditions, from the IL solution, CoPt deposits with 72.6 at. % of Co and 27.4 at. % of Pt composition, and a porous morphology (Figure 2b) were obtained, although at a very low deposition rate (24 nm·h^{-1}). From the IL-S system, the deposition was also possible but at an even lower deposition rate (1.2 nm·h^{-1}) leading to a quasi-continuous (Figure 2c) morphology with very small grains. This morphology could be explained by the capability of surfactants to keep the interfacial surface tension over the growing electrode surface. This produces an organized deposition of adatoms on the proper sites of the surface producing a compact deposit,

with enhanced adhesion to the substrate. In this case, the obtained deposits contain 74.9 at. % of Co and 25.1 at. % of Pt. Therefore, non-significant changes in composition were observed with respect to the pure IL case.

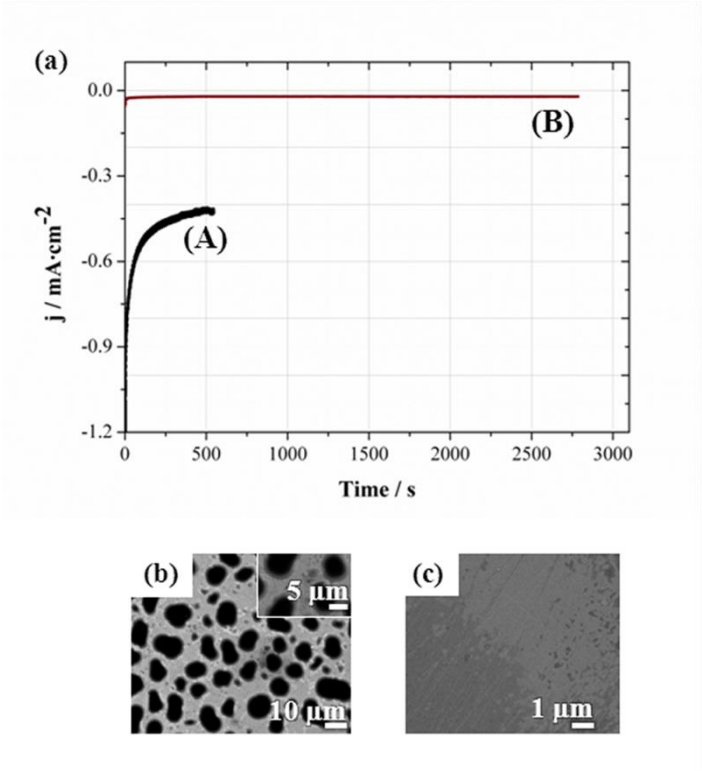

Figure 2: Cronoamperometric curves (a) and SEM images (b, c) of the CoPt deposit obtained at -1.75 V on the Si/Ti (15 nm)/Au (100 nm) substrate at 25 ºC after circulating (a-A, b) 100 mC·cm^{-2} in a 1.2 mM Na_2PtCl_6 + 2.5 mM $CoCl_2$ solution in the IL and (a-B, c) 50 mC·cm^{-2} in IL-S system containing 59.4 wt. % of 1.2 mM Na_2PtCl_6 and 2.5 mM $CoCl_2$ in IL solution and 40.6 wt. % of Triton X-100.

The electrodeposition tests clearly show that only a low proportion of the electroactive species (Co(II) and Pt(IV)) can be dissolved in the bmimPF_6 IL (and only after two days of solubilisation). The results of the tests performed with these IL solutions (with and without surfactant) reveal that deposition of the alloy is possible but at very negative potentials and with very low deposition rates, especially in the presence of the surfactant. Consequently, since after the preparation of the W/IL microemulsions, the Pt (IV) and Co (II) salts will be present mainly in the aqueous component of the microemulsions, we expect that the CoPt electrodeposition will

take place mainly from the aqueous component, even if a small amount of Pt (IV) and Co (II) were present in the IL component.

Electrochemical Synthesis of Magnetic CoPt Nanoparticles in W/IL Microemulsions

In this section, we analyze the electrochemical synthesis of magnetic CoPt nanoparticles in W/IL microemulsions, illustrated schematically in Figure 3a. Microemulsions (Table 1) with different aqueous content, at constant surfactant-ionic liquid ratio ($R_{S:IL}$) (microemulsions I, II and III), and different surfactant content, at constant aqueous content (microemulsions I and IV), have been considered to control the droplet size and ionic conductivity.

TABLE 1: Considered microemulsion systems.

Microemulsion system	$R_{S:IL}$	[W] / wt. %	Conductivity [a] / $\mu S \cdot cm^{-1}$
I	4.1	7.40	335
II	4.1	16.6	625
III	4.1	26.0	1147
IV	0.78	7.40	45

[a] Note that the conductivity of the pure components, *i.e.*, aqueous solution, the bmimPF6 ionic liquid and Triton X-100 surfactant, are 10840, 275, 1.57 $\mu S \cdot cm^{-1}$, respectively.

Figure 3b, 3c show cyclic voltamograms of the different W/IL microemulsion systems. Notably, in these W/IL/S systems some differences were observed with respect to the voltammetric profile in the simple CoPt-IL solutions (Figure 1). Pt deposition occurs now during the first wide reduction peak as in pure aqueous solutions, followed by the reduction of the protons over the previously deposited Pt and the simultaneous cobalt deposition. The CoPt alloy oxidation peak around -0.3 V is detected, after which both Au and Pt surface oxidation is detected in the second oxidation peak. Hence, the voltammetric curves show a similar profile than those detected in CoPt/aqueous solution[47, 48] but with a lower current density due to the low proportion of aqueous component. Therefore, these results confirm that CoPt electrodeposition

takes place in the aqueous component medium rather than from the IL. Figure 3b (microemulsions I, II and III) analyzes the effect of the aqueous content, at constant $R_{S:IL}$, on the electrochemical process. The results demonstrate a higher current density and higher CoPt alloy oxidation peak (first oxidation peak) when the aqueous content increases due to the lower ohmic resistance of the medium (Table 1). Figure 3d (microemulsions I and IV) shows that different surfactant proportion also affects the deposition rate.

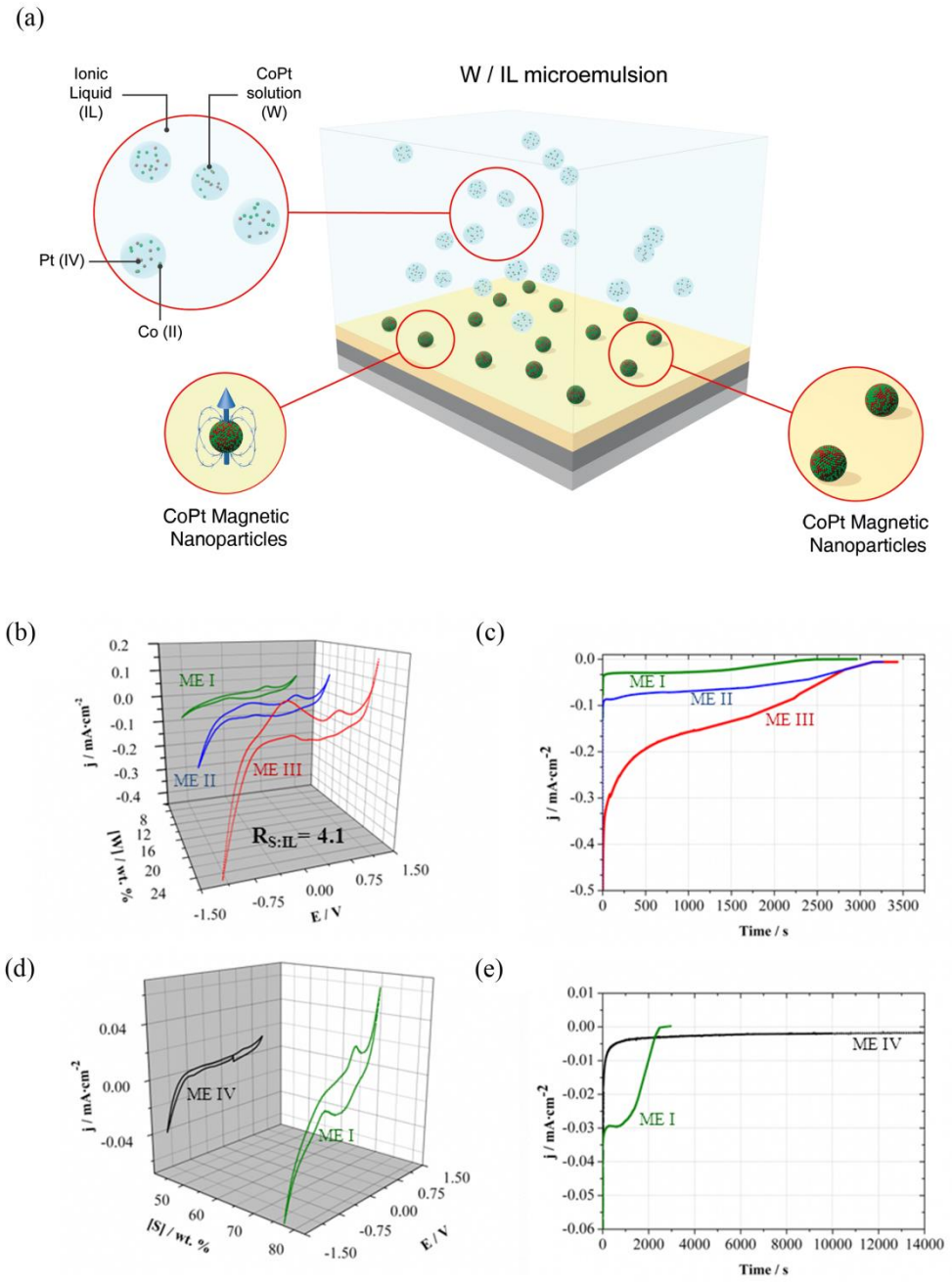

Figure 3: (a) Schematic representation of electrochemical synthesis of magnetic CoPt nanoparticles in W/IL microemulsions. Cyclic voltammetry under stationary conditions at 50 $mV \cdot s^{-1}$ of (b) microemulsions I, II and III, and (d microemulsions I and IV. Cronoamperometric curves of the CoPt deposit obtained at -1.05 V (c) microemulsions I, II and III, and (e) microemulsions I and IV.

Based on the voltammetry curves, CoPt deposits were prepared, from IL/W microemulsions at potentials at which Pt and Co codeposition was possible. The cronoamperometric curves (Figure 3c and 3e) show different deposition rate for each microemulsion. Namely, the current density increases by increasing the percentage of aqueous solution in the microemulsion (Figure 3c). In all cases, the current density decreases at long deposition times and tends asymptotically to zero due to the consumption of the electroactive species inside the droplets.

TEM micrographs (Figure 4), after detaching deposits from the substrate, show that the electrochemical process from the W/IL/S microemulsions renders spherical nanoparticles with well-defined sizes. Importantly, the nanoparticle size increases as the aqueous content increases, at constant $R_{S:IL}$, as expected according to the electrochemical analysis. Namely, microemulsions I and IV, with 7.4% of aqueous solution, render small particles 14-17 nm in diameter with a rather narrow particle size distribution; while microemulsion II and III (with 16 and 26.6 % of aqueous solution, respectively) give rise to considerably larger nanoparticles with 40 and 95 nm in size, and a somewhat larger particle size distribution.

High resolution TEM (HR-TEM) images (Figure 4d2), with clear lattice fringes demonstrate the good crystalline quality of the samples. The fast Fourier transform of the lattice fringes in the HR-TEM and the selected area diffraction patterns (see insets in Figure 4c, 4d1) allow us to identify the structure of the nanoparticles as a distorted hcp structure.[47-49] Note that this CoPt structure has been obtained in electrochemical CoPt deposits for Co-rich alloys.[47-49] Moreover, some cobalt oxides (Co_3O_4) were also detected, as expected from the surface oxidation of the particles when exposed to air.

The homogenous sizes obtained from TEM indicate that droplets of the aqueous solutions act as nanoreactors in which the electrochemical reduction takes place, thus serving as

nanotemplates for the growth of the nanoparticles. Due to the template character of the nanoreactors, increasing the amount of aqueous solution in the ionic liquid increases the size of these nanoreactors and consequently leads to larger particles, confirming that the size of the droplets determines the final size and size distribution of the particles. In fact, this method presents significant advantage with respect to chemical synthesis of nanoparticles in microemulsions, since it allows controlling the nanoparticle size over a very broad range, from few nanometers to over hundred nanometers.

As can be seen in Table 2, the CoPt deposition rate was appreciably low (5 - 150 $nm \cdot h^{-1}$) with respect to that in pure CoPt aqueous solution (2760 $nm \cdot h^{-1}$). Nevertheless, it is considerably larger than in the IL and in IL-S media without microemulsions. Thus, the alloy deposits from the droplets of the aqueous component due to the low solubility of the electroactive species in the IL and the extremely low deposition rate from the IL solution in the presence of surfactant. Hence, W/IL/S microemulsions offer clear advantages over classical water-in-oil microemulsions as a soft template for electrodeposition due to the substitution of oil (dielectric) by a more conductive component (IL) if the electroactive species present a low solubility in the IL medium. Moreover, these W/IL/S microemulsions can be used as a more efficient alternative to the W/O/S microemulsions proposed for template electrodeposition of alloys[31–33] because since their improved conductivity substantially increases the deposition rate.

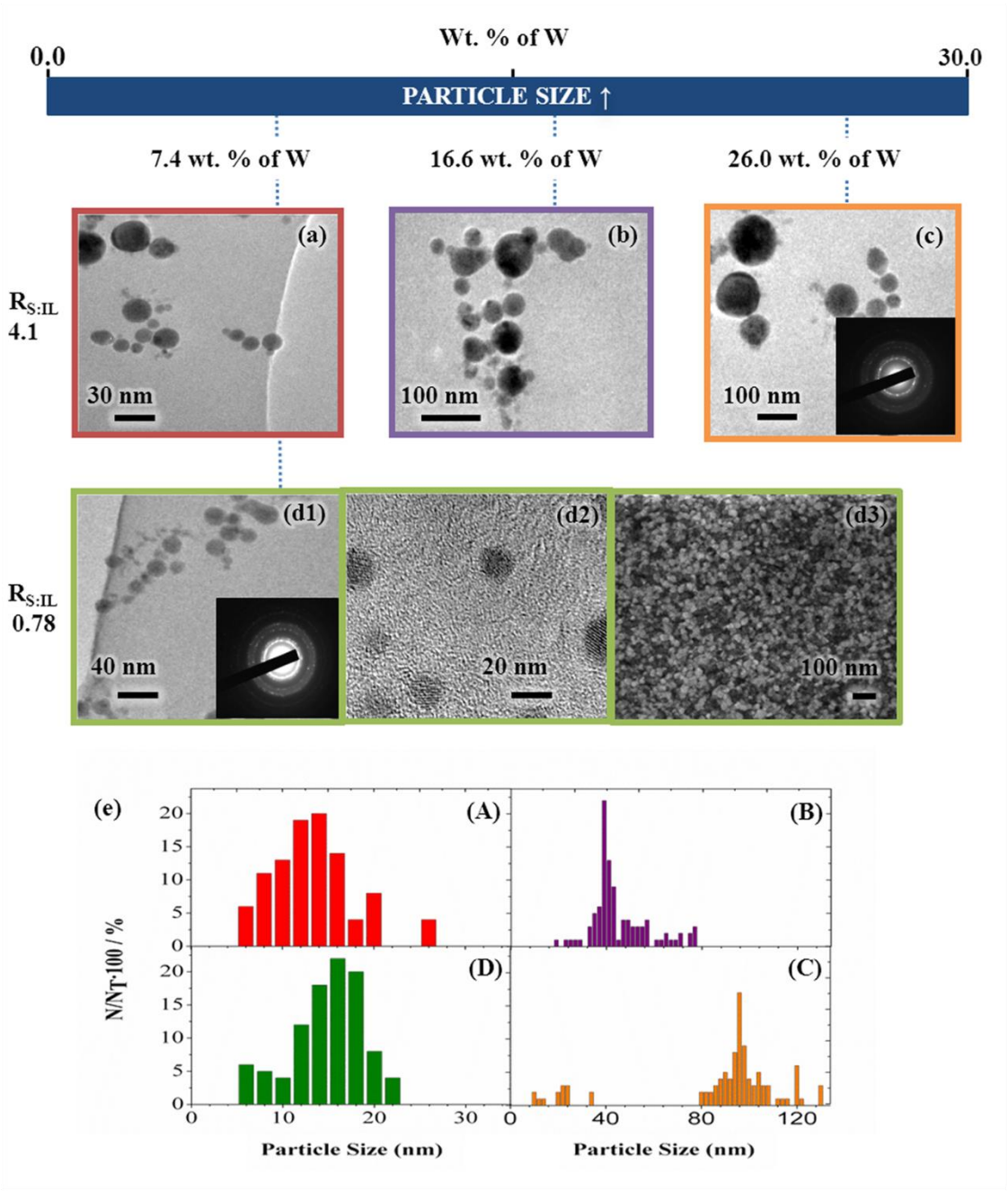

Figure 4: Transmission electron micrographs (a, b, c, d), particle size distribution (e.A, e.B, e.C, e.D), high-resolution transmission electron micrograph (d2), and field-emission electron scanning micrograph (d3) of CoPt deposits prepared at -1.05 V W/IL microemulsions (a) I, (b) II, (c) III, and (d1) IV. Insets in Transmission electron micrograph (c, d) correspond to representative selected area electron diffraction patterns.

Table 2 summarizes the composition of the CoPt nanoparticles and the effective thickness of the layer of nanoparticles for microemulsions I-IV at -1.05 V and for microemulsion III at the different selected potentials.

TABLE 2: Composition, effective thickness and deposition rate of the deposits obtained through the j-t transients of Figure 3.

Microemulsion system	Potential / V	Circulated charge density / $mC \cdot cm^{-2}$	Pt / at. %	Co / at. %	Effective thickness / nm	Deposition rate / $nm \cdot h^{-1}$
I	-1.05	100	32.5	67.5	15	18
II	-1.05	200	33.5	66.5	40	45
IIIa	-1.05	600	31.7	68.3	98	101
IV	-1.05	100	34.1	65.9	18	5
IIIa	-1.05	600	31.7	68.3	98	101
IIIb	-1.10	600	31.8	68.2	98	130
IIIc	-1.15	600	33.5	66.5	95	150

It can be seen from Table 2 that the effective thickness coincides with the particle size obtained from TEM. This implies that that nanoparticles form single monolayers of CoPt nanoparticles on the substrate as evidenced by field-emission scanning electron microscopy (Figure 4d2).

Remarkably, the CoPt stoichiometry of the nanoparticles remains virtually constant ($Co_{67\pm1}Pt_{33\pm1}$) for the diverse conditions studied (Table 2). Moreover, the composition is essentially identical to the relative atomic percentages of Co(II) and Pt(IV) in the aqueous solution component of the microemulsion, *i.e.*, 67.6 at. % of Co and 32.4 at. % of Pt. Thus, the stoichiometry of the alloyed nanoparticles does not depend on the amount of aqueous solution or the electrochemical potential. Accordingly, the composition of the CoPt nanoparticle

accurately replicates the relative proportion of the Co and Pt in the aqueous solution of the droplets, confirming once more that the deposition stems directly from the aqueous droplets.

To further confirm the correlation between the composition of the droplets and the stoichiometry of the nanoparticles we have electrodeposited W/IL/S microemulsions where the composition has been altered by increasing the amount of $CoCl_2$ from 2.5 mM to 7.5 mM using the conditions of microemulsion IIIa.

TABLE 3: Composition of the aqueous solution and the nanoparticles for different $CoCl_2/Na_2PtCl_6$ rations in the solution.

Composition of the aqueous solution	Composition of the nanoparticles
67.6 at. % of Co 32.4 at. % of Pt	$Co_{66.5}Pt_{33.5}$
79.9 at. % of Co 20.1 at. % of Pt	$Co_{80.6}Pt_{19.4}$
86.2 at. % of Co 13.8 at. % of Pt	$Co_{87.5}Pt_{12.5}$

As can be seen in Table 3, the composition of the nanoparticles reliably reproduces the one of the aqueous solution for all the conditions studied. Moreover, the size of the nanoparticles (not shown) remains virtually the same for the different compositions. These results confirm once more that the deposition occurs directly from the aqueous solution in the nanoreactors and that no significant contribution from any deposition from the IL can be observed. Thus, an unprecedented control not only over the size of the nanoparticles, but also over the composition can be easily achieved in alloyed nanoparticles using W/IL/S microemulsions. The method allows obtaining alloy nanoparticles in a wide range of sizes in the nanometer range and with an easily adjusted composition.

As can be seen in Figure 5, the magnetic properties of the nanoparticles depend strongly on their size. The small CoPt nanoparticles (17 nm, microemulsion IV) exhibit a

superparamagnetic behavior at room temperature, with vanishing remananece and coercivity.[50] Namely, given the small size of the nanoparticles and the moderate anisotropy of the CoPt alloys in the hcp structure[51-54] the blocking temperature of the material lays below room temperature. On the other hand, the large particles (90 nm, microemulsion III) show a hard magnetic behavior with a rather large coercivity, H_C = 4100 Oe and a remanence-to-saturation ratio, M_R/M_S ~ 0.52. This M_R/M_S value is the one expected for non-interacting nanoparticles with uniaxial anisotropy with a random distribution of easy axes.[55] This H_C is consistent with the reported anisotropy of hcp CoPt films (~10^7 erg/cm^3)[51-54] and in line with H_C values of hcp CoPt films and microstructures of similar compositions.[51-54, 56, 57] Interestingly, these attractive magnetic properties are observed in the as-obtained state, *i.e.*, without the need of any post-annealing. This is in contrast to many hard magnetic alloys were high temperature treatments are necessary to establish the hard phase, *e.g.* $L1_0$ FePt.[58] Consequently, hcp CoPt alloys are emerging as an appealing alternative to other hard magnetic alloys for magnetic recording or magnetically actuated microelectromechanical systems (MEMS) applications.[51, 56, 57] Moreover, hard magnetic nanoparticles can be interesting for patterned recording media or as building blocks for permanent magnets.[58, 59]

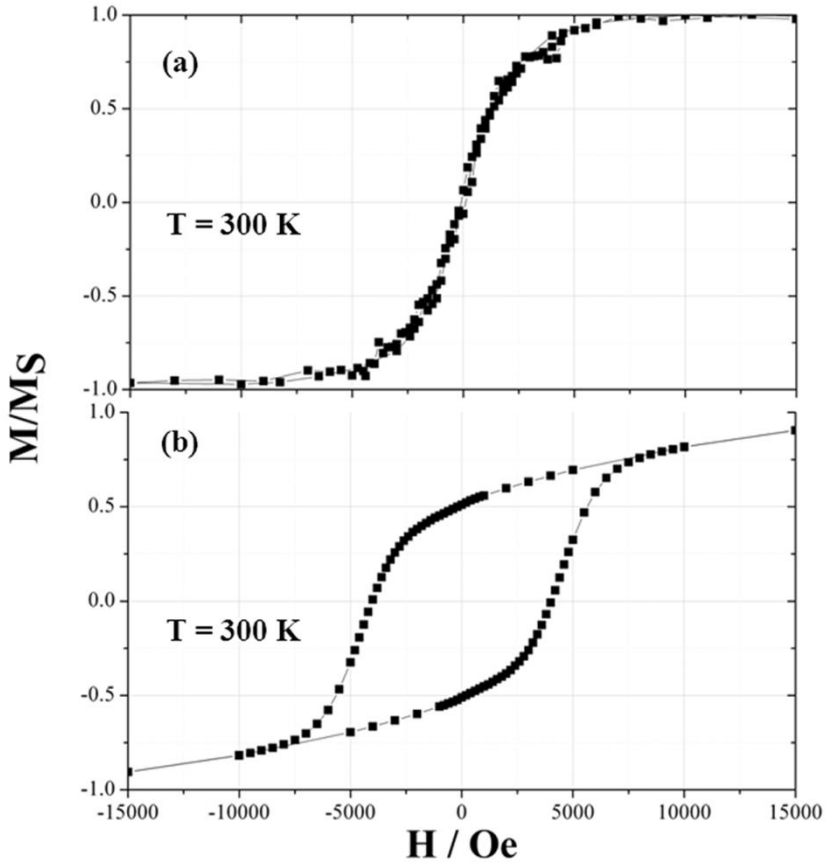

Figure 5: Room temperature in-plane hysteresis loop of CoPt nanoparticles obtained in microemulsion (a) IV and (b) III.

CONCLUSIONS

Electrochemical reduction from water-in-ionic liquid microemulsions is established as a very versatile synthesis approach to grow alloy nanoparticles of different sizes and compositions in a green, simple, inexpensive way. The advantage of the process relies on the (i) droplets of aqueous solution in the microemulsions acting as nanotemplates for nanoparticle growth, which allows the reliable control over sizes and compositions and (ii) the higher conductivity of the ionic liquid over other electrochemical media, which leads to reasonable deposition rates. The method allows preparing hcp $Co_{1-x}Pt_x$ nanoparticles over a broad size range, 10-120 nm, with tuneable compositions (Co 66-88 at % - Pt 33-12 at %) on conductive substrates, by controlling the proportion and composition of the aqueous component, containing Pt and Co ions, in the

microemulsion. The size and the hcp character of the nanoparticles leads to varying magnetic behaviours ranging from superparamagnetism to hard-magnetism with moderately large coercivities.

METHODS

Microemulsion Preparation and Materials.

The ionic liquid microemulsion was prepared by mixing of aqueous component (W), Triton X-100 (S) and bmimPF_6 (IL) in different proportions.[41,42] The mixture was sonicated during 5 minutes under argon bubbling, leading to transparent and stable microemulsions.

- Non-ionic surfactant (S) (p-octyl polyethylene glycol phenyl ether *a.k.a*. Triton X-100 – Acros Organics, 98 %–).

- Ionic liquid (IL) (1-Butyl-3-methylimidazolium hexafluorophosphate *a.k.a*. bmimPF_6 – Arcos Organics, > 98 %–).

- Co-Pt aqueous solution (W). The aqueous solution contains 2.5 mM $CoCl_2$, 1.2 mM Na_2PtCl_6, 0.1 M NH_4Cl, 10 $g \cdot dm^{-3}$ H_3BO_3 at a pH adjusted to pH = 4.5 with NaOH solutions. Reagents used were Co (II) chloride (Carlo Erba, > 98.0 %), sodium hexacloroplatinate (IV) hexahydrate (Aldrich, 98 %), Ammonium chloride (Fluka, > 99.5 %), Boric acid (Merck, 99.8 %) and deionized water (Millipore Q-System) with resistivity of 18.2 $M\Omega \cdot cm^{-1}$.

Electrochemical Study and Characterization.

The electrochemical study of the deposition process was performed at room temperature (25ºC) using a three-electrode electrochemical system with Si/Ti (15 nm)/Au (100 nm) substrates (0.5 cm x 0.5 cm), Pt spiral, and Ag / AgCl /1 M KCl as working, counter, and reference electrodes, respectively. A microcomputer controlled potentiostat/galvanostat Autolab with PGSTAT30 equipment and GPES software was used. The system was de-aerated before each experiment by argon bubbling. Importantly, none of the systems were stirred during the

electrodeposition process to maintain the structure of microemulsion during the deposition process.

The morphology and structure of the deposited CoPt nanoparticles were examined by using Transmission Electron Microscopy (Hitachi 800 MT and JEOL 2100). For the TEM analysis it is essential to release the nanostructures from the substrate. This was achieved by removing the Au layer using a saturated I_2/I^- solution. The nanostructures were later retained by an external magnetic field and washed with water and ethanol and deposited on carbon grids. Elemental composition and effective thickness were measured using an electron probe micro-analysis (EPMA) by wavelength-dispersive x-ray spectroscopy analysis (WDS) equipped with a Camera SX-50 equipment.

The magnetic characterization of the deposits was carried out by using a superconducting quantum interference device (SQUID) magnetometer (Quantum Design MPMS-XL). Hysteresis loops, with a maximum applied field of 7 T, were measured at room temperature with the field applied in the film plane. Note that a diamagnetic linear background, corresponding to the substrate and buffer layers, has been subtracted from the data.

ACKNOWLEDGMENT:

This work was supported by contracts CQT2010-20726 and MAT2010-20616-C02 from MINECO and project 2009-SGR-1292 from the Generalitat de Catalunya. The authors wish to thank the Centres Científics i Tecnològics de la Universitat de Barcelona (CCiTUB) for allowing us to use their equipment. Substrates have been prepared in IMB-CNM (CSIC), supported by the (CSIC) NGG-258 project. A.S. would also like to thank the Ministerio de Educación, Cultura y Deporte for its financial support (FPU grant).

REFERENCES:

(1) Haruta, M.; Daté, M. Advances in the Catalysis of Au Nanoparticles. *Appl. Catal. A Gen.* **2001**, *222*, 427–437.

(2) Astruc, D.; Lu, F.; Aranzaes, J. R. Nanoparticles as Recyclable Catalysts: The Frontier between Homogeneous and Heterogeneous Catalysis. *Angew. Chem. Int. Ed.* **2005**, *44*, 7852–7872.

(3) Wang, F.; Banerjee, D.; Liu, Y.; Chen, X.; Liu, X. Up Conversion Nanoparticles in Biological Labeling, Imaging, and Therapy. *Analyst* **2010**, *135*, 1839–1854.

(4) Pan, Y.; Shan, W.; Fang, H.; Guo, M.; Nie, Z.; Huang, Y.; Yao, S. Sensitive and Visible Detection of Apoptotic Cells on Annexin-V Modified Substrate Using Aminophenylboronic Acid Modified Gold Nanoparticles (APBA-GNPs) labeling. *Biosens. Bioelectron.* **2013**, *52C*, 62–68.

(5) Roy, I.; Ohulchanskyy, T. Y.; Pudavar, H. E.; Bergey, E. J.; Oseroff, A. R.; Morgan, J.; Dougherty, T. J.; Prasad, P. N. Ceramic-Based Nanoparticles Entrapping Water-Insoluble Photosensitizing Anticancer Drugs: A Novel Drug-Carrier System for Photodynamic Therapy. *J. Am. Chem. Soc.* **2003**, *125*, 7860–7865.

(6) Jin, Y.; Wang, J.; Sun, B.; Blakesley, J. C.; Greenham, N. C. Solution-Processed Ultraviolet Photodetectors Based on Colloidal ZnO Nanoparticles. *Nano Lett.* **2008**, *8*, 1649–1653.

(7) Choi, H.; Ko, S.-J.; Choi, Y.; Joo, P.; Kim, T.; Lee, B. R.; Jung, J.-W.; Choi, H. J.; Cha, M.; Jeong, J.-R.; *et al.* Versatile Surface Plasmon Resonance of Carbon-Dot-Supported Silver Nanoparticles in Polymer Optoelectronic Devices. *Nat. Photonics* **2013**, *7*, 732–738.

(8) Liu, Y.; Sun, X.; Wang, S.; Xie, M.; Chen, A.; Long, R. Preparation of Nanoparticles Embedded Microcapsules (NEMs) and Their Application in Drug Release. *Mater. Lett.* **2012**, *75*, 48–50.

(9) Katz, E.; Willner, I. Integrated Nanoparticle–Biomolecule Hybrid Systems: Synthesis, Properties, and Applications. *Angew. Chem. Int. Ed.* **2004**, *43*, 6042–6108.

(10) Katz, E.; Willner, I. A Quinone-Functionalized Electrode in Conjunction with Hydrophobic Magnetic Nanoparticles Acts as a ‘‘Write–Read–Erase’’ Information Storage System. *Chem. Commun. (Camb).* **2005**, 5641–5643.

(11) Lee, J.-S.; Kim, Y.-M.; Kwon, J.-H.; Sim, J. S.; Shin, H.; Sohn, B.-H.; Jia, Q. Multilevel Data Storage Memory Devices Based on the Controlled Capacitive Coupling of Trapped Electrons. *Adv. Mater.* **2011**, *23*, 2064–2068.

(12) Ahmadi, T.; Wang, Z.; Green, T.; Henglein, A; El-Sayed, M. Shape-Controlled Synthesis of Colloidal Platinum Nanoparticles. *Science* **1996**, *272*, 1924–1926.

(13) Mock, J. J.; Barbic, M.; Smith, D. R.; Schultz, D. A.; Schultz, S. Shape Effects in Plasmon Resonance of Individual Colloidal Silver Nanoparticles. *J. Chem. Phys.* **2002**, *116*, 6755-6759.

(14) Chithrani, B. D.; Chan, W. C. W. Elucidating the Mechanism of Cellular Uptake and Removal of Protein-Coated Gold Nanoparticles of Different Sizes and Shapes. *Nano Lett.* **2007**, *7*, 1542–1550.

(15) Bajaj, G.; Soni, R. K. Effect of Liquid Medium on Size and Shape of Nanoparticles Prepared by Pulsed Laser Ablation of Tin. *Appl. Phys. A* **2009**, *97*, 481–487.

(16) Ning, J.; Men, K.; Xiao, G.; Wang, L.; Dai, Q.; Zou, B.; Liu, B.; Zou, G. Facile Synthesis of IV–VI SnS Nanocrystals with Shape and Size Control: Nanoparticles, Nanoflowers and Amorphous Nanosheets. *Nanoscale* **2010**, *2*, 1699–1703.

(17) Powers, K. W.; Palazuelos, M.; Moudgil, B. M.; Roberts, S. M. Characterization of the Size, Shape, and State of Dispersion of Nanoparticles for Toxicological Studies. *Nanotoxicology* **2007**, *1*, 42–51.

(18) Wu, M.-L.; Chen, D.-H.; Huang, T.-C. Preparation of Pd/Pt Bimetallic Nanoparticles in Water/AOT/Isooctane Microemulsions. *J. Colloid Interface Sci.* **2001**, *243*, 102–108.

(19) Santra, S.; Tapec, R.; Theodoropoulou, N.; Dobson, J.; Hebard, A.; Tan, W. Synthesis and Characterization of Silica-Coated Iron Oxide Nanoparticles in Microemulsion: The Effect of Nonionic Surfactants. *Langmuir* **2001**, *17*, 2900–2906.

(20) Zarur, A.; Ying, J. Reverse Microemulsion Synthesis of Nanostructured Complex Oxides for Catalytic Combustion. *Nature* **2000**, *403*, 65–67.

(21) Mojahedian, M. M.; Daneshamouz, S.; Samani, S.M.; Zargaran, A. A Novel Method to Produce Solid Lipid Nanoparticles Using N-butanol as an Additional Co-surfactant Cccording to the O/W Microemulsion Quenching Technique. *Chem. Phys. Lipids* **2013**, *174*, 32-38.

(22) Capek, I. Preparation of Metal Nanoparticles in Water-in-Oil (w/o) Microemulsions. *Adv. Colloid Interface Sci.* **2004**, *110*, 49–74.

(23) Sjiiblom, J.; Lindbergh, R.; Fribergc, S. E. Microemulsions-Phase Equilibria Characterization, Structures, Applications and Chemical Reactions. *Adv. Colloid Interface Sci.* **1996**, *95*, 125–287.

(24) Chen, D.; Wu, S. Synthesis of Nickel Nanoparticles in Water-in-Oil Microemulsions. *Chem. Mater.* **2000**, 13, 1354–1360.

(25) Kitchens, C. L.; McLeod, M. C.; Roberts, C. B. Chloride Ion Effects on Synthesis and Directed Assembly of Copper Nanoparticles in Liquid and Compressed Alkane Microemulsions. *Langmuir* **2005**, *21*, 5166–5173.

(26) Teo, B. M.; Ashokkumar, M.; Grieser, F. Microemulsion Polymerizations *via* High-Frequency Ultrasound Irradiation. *J. Phys. Chem. B* **2008**, *112*, 5265–5267.

(27) Najjar, R.; Stubenrauch, C. Phase Diagrams of Microemulsions Containing Reducing Agents and Metal Salts as Bases for the Synthesis of Metallic Nanoparticles. *J. Colloid Interface Sci.* **2009**, *331*, 214–220.

(28) Note, C.; Kosmella, S.; Koetz, J. Poly(ethyleneimine) as Reducing and Stabilizing Agent for the Formation of Gold Nanoparticles in W/O Microemulsions. *Colloids Surf. A Physicochem. Eng. Asp.* **2006**, *290*, 150–156.

(29) Serrà, A.; Gómez, E.; Calderó, G.; Esquena, J.; Solans, C.; Vallés, E. Microemulsions for Obtaining Nanostructures by Means of Electrodeposition Method. *Electrochem. Commun.* **2013**, *27*, 14–18.

(30) Serrà, A.; Gómez, E.; Calderó, G.; Esquena, J.; Solans, C.; Vallés, E. Conductive Microemulsions for Template CoNi Electrodeposition. *Phys. Chem. Chem. Phys.* **2013**, *15*, 14653–14659.

(31) Ganesh, V.; Lakshminarayanan, V. Microemulsion Phase as a Medium for Electrodeposition of Nickel and Electron-Transfer Study of Ferrocyanide–Ferricyanide Redox System. *J. Colloid Interface Sci.* **2010**, *349*, 300–306.

(32) Endres, F. Ionic Liquids: Solvents for the Electrodeposition of Metals and Semiconductors. *ChemPhysChem* **2002**, *3*, 144–154.

(33) Abbott, A. P.; McKenzie, K. J. Application of Ionic Liquids to the Electrodeposition of Metals. *Phys. Chem. Chem. Phys.* **2006**, *8*, 4265–4279.

(34) He, P.; Liu, H.; Li, Z.; Li, J. Electrodeposition of Platinum in Room-Temperature Ionic Liquids and Electrocatalytic Effect on Electro-oxidation of Methanol. *J. Electrochem. Soc.* **2005**, *152*, E146-E153.

(35) Eastoe, J.; Gold, S.; Rogers, S. E.; Paul, A.; Welton, T.; Heenan, R. K.; Grillo, I. Ionic Liquid-in-Oil Microemulsions. *J. Am. Chem. Soc.* **2005**, *127*, 7302–7303.

(36) Gao, H.; Li, J.; Han, B.; Chen, W.; Zhang, J.; Zhang, R.; Yan, D. Microemulsions with Ionic Liquid Polar Domains. *Phys. Chem. Chem. Phys.* **2004**, *6*, 2914-2916.

(37) Yan, F.; Texter, J. Surfactant Ionic Liquid-Based Microemulsions for Polymerization. *Chem. Commun.* **2006**, 2696–2698.

(38) Fu, C.; Zhou, H.; Xie, D.; Sun, L.; Yin, Y.; Chen, J.; Kuang, Y. Electrodeposition of Gold Nanoparticles from Ionic Liquid Microemulsion. *Colloid Polym. Sci.* **2010**, *288*, 1097–1103.

(39) Fu, C.; Zhou, H.; Peng, W.; Chen, J.; Kuang, Y. Comparison of Electrodeposition of Silver in Ionic Liquid Microemulsions. *Electrochem. Commun.* **2008**, *10*, 806–809.

(40) Gao, Y.; Wang, S.; Zheng, L.; Han, S.; Zhang, X.; Lu, D.; Yu, L.; Ji, Y.; Zhang, G. Microregion Detection of Ionic Liquid Microemulsions. *J. Colloid Interface Sci.* **2006**, *301*, 612–616.

(41) Gao, Y.; Han, S.; Han, B.; Li, G.; Shen, D.; Li, Z.; Du, J.; Hou, W.; Zhang, G. TX-100/Water/1-Butyl-3-methylimidazolium Hexafluorophosphate Microemulsions. *Langmuir* **2005**, *21*, 5681–5684.

(42) Li, N.; Gao, Y.; Zheng, L.; Zhang, J.; Yu, L.; Li, X. Studies on the Micropolarities of bmimBF4/TX-100/Toluene Ionic Liquid Microemulsions and Their Behaviors Characterized by UV-Visible Spectroscopy. *Langmuir* **2007**, *23*, 1091–1097.

(43) Gómez, E.; Vallés, E. *Int.* Platinum Electrodeposition in an Ionic Liquid Analogue. Solvent Stability Monitoring. *J. Electrochem. Sci.* **2013**, *8*, 1443–1458.

(44) Luo, B.; Li, X.; Li, X.; Xue, L.; Li, S.; Li, X. Copper Nanocubes and Nanostructured Cuprous Oxide Prepared by Surfactant-assisted Electrochemical Deposition. *CrystEngComm* **2013**, *15*, 5654-5659.

(45) Guo, C.; Zuo, Y.; Zhao, X.; Zhao, J.; Xiong, J. Effects of Surfactants on Electrodeposition of Nickel-Carbon Nanotubes Composite Coatings. *Surf. Coat. Technol.* **2008**, *202*, 3385–3390.

(46) Chen, L.; Wang, L.; Zeng, Z.; Zhang, J. Effect of Surfactant on the Electrodeposition and Wear Resistance of Ni–Al_2O_3 Composite Coatings. *Mater. Sci. Eng. A* **2006**, *434*, 319–325.

(47) Cortés, M.; Serrà, A.; Gómez, E.; Vallés, E. CoPt Nanoscale Structures with Different Geometry Prepared by Electrodeposition for Modulation of Their Magnetic Properties. *Electrochim. Acta* **2011**, *56*, 8232–8238.

(48) Grau, S.; Montiel, M.; Gómez, E.; Vallés, E. Ternary PtCoNi Functional Films Prepared by Electrodeposition: Magnetic and Electrocatalytic Properties. *Electrochim. Acta* **2013**, *109*, 187–194.

(49) Cortés, M.; Gómez, E. Vallés, E. Magnetic Properties of Nanocrystalline CoPt Electrodeposited Films. Influence of P Incorporation. *J. Solid State Electrochem.* **2010**, *14*, 2225-2233.

(50) Knobel, M.; Nunes, W.C.; Socolovsky, L.M.; De Biasi, E.; Vargas, J.M.; Denardin, J.C. Superparamagnetism and Other Magnetic Features in Granular Materials: A Review on Ideal and Real Systems. *J. Nanosci. Nanotechnol.* **2008**, *8*, 2836-2857.

(51) Nozawa, N.; Siato, S.; Hinata, S.; Takahashi, M. Large Uniaxial Magnetocrystalline Anisotropy for $Co_{50}Pt_{50}$ Disordered Alloy Films with Hexagonal-Close-Packed Stacking Structure by Substituting Pt with Rh. *J. Phys D* **2013**, *46*, 172001-172001.

(52) Bolzoni, F.; Leccabue, F.; Panizzieri, R.; Pareti, L. Magnetocrystalline Anisotropy and Phase Transformation in Co-Pt alloy. *IEEE Trans. Magn.* **1984**, *20*, 1625-1627.

(53) Pattanaik, G.; Zangari,G.; Weston, J. Perpendicular Anisotropy in Electrodeposited, Co-Rich Co-Pt Films by Use of Ru Underlayers. *Appl. Phys. Lett.* **2006**, *89*, 112506-112509.

(54) Zana, I.; Zangari, G. Magnetic Properties of Electrodeposited Co-Pt Thin Films with Very High Perpendicular Magnetic Anisotropy. *J. Magn. Magn. Mater.* **2004**, *272-276*, 1698-1699.

(55) Stoner, E. C.; Wohlfarth, E. P. *Philos. Trans. R. Soc. London Ser. A* **1948**, *240*, 599-642.

(56) Zana, I.; Zangari, G.; Park, J. W.; Allen, M.G. Electrodeposited Co-Pt Micron-Size Magnets with Strong Perpendicular Magnetic Anisotropy for MEMS Applications. *J. Magn. Magn. Mater.* **2004**, *272-276*, e1775–e1776.

(57) Wang, N. G.; Arnold, D.P. Thick Mlectroplated Co-rich Co–Pt Micromagnet Arrays for Magnetic MEMS. *IEEE Trans. Magn.* **2008**, *44*, 3969-3972.

(58) Poudyal, N.; Liu, J.P. Advances in Nanostructured Permanent Magnets Research. *J. Phys. D* **2013**, *46*, 043001-043024.

(59) Terris, B.D; Thomson, T. Nanofabricated and Self-Assembled Magnetic Structures as Data Storage Media. *J. Phys. D* **2005**, *38*, R199-R222